

PAPER

In situ Kerr and harmonic measurement in determining current-induced effective fields in MgO/CoFeB/Ta

To cite this article: Q Y Wong *et al* 2018 *J. Phys. D: Appl. Phys.* **51** 115004

View the [article online](#) for updates and enhancements.

Related content

- [Spin-orbit torque switching in MgO/CoFeB/Ta/CoFeB/MgO heterostructures with a critical current density of \$10^9\$ A/cm²](#)
Guoyi Shi, Yuansi Chang, Jianwang Cai *et al.*
- [Current-induced magnetization switching in Pt/Co/Ta with interfacial decoration by insertion of Cr to enhance perpendicular magnetic anisotropy and spin-orbit torques](#)
Baoshan Cui, Shiwei Chen, Dong Li *et al.*
- [Spin-orbit torques and magnetization switching in W/Co₂FeAl/MgO structures](#)
M S Gabor, T Petrisor Jr, R B Mos *et al.*



LIVE WEBINAR

NanoRaman: Correlated Tip-Enhanced Optical Spectroscopy and Scanning Probe Microscopy

Thursday 8 March 15.00 GMT

REGISTER NOW!

physicsworld.com

In situ Kerr and harmonic measurement in determining current-induced effective fields in MgO/CoFeB/Ta

Q Y Wong[✉], W L Gan[✉], F L Luo, G J Lim[✉], C C I Ang[✉], F N Tan[✉],
W C Law[✉] and W S Lew[✉]

School of Physical and Mathematical Sciences, Nanyang Technological University, 21 Nanyang Link, 637371, Singapore

E-mail: wensiang@ntu.edu.sg

Received 10 January 2018, revised 31 January 2018

Accepted for publication 13 February 2018


Published 23 February 2018



Abstract

A combination of the harmonic measurement and *in situ* Kerr imaging was used to experimentally determine the spin-orbit (SO) effective fields in a MgO/CoFeB/Ta structure. Here, we evaluate the SO effective fields through an analytical energy approach by transforming the anomalous Hall effect and planar Hall effect (PHE) voltage into a field dependency while imaging the magnetisation behaviour by differential Kerr microscopy. The analytical fitting to the measurement data indicates the significant coexistence of both a transverse field, H_T , and longitudinal field, H_L , in the longitudinal ($H_L = -12$ Oe, $H_T = 8$ Oe per 10^6 A cm⁻²) and transverse ($H_L = -12$ Oe, $H_T = -17$ Oe per 10^6 A cm⁻²) measurement schemes, respectively, due to the PHE. Additionally, dendritic-like domains, indicating the influence of the interfacial Dzyaloshinskii-Moriya interaction (DMI) at the CoFeB/Ta interface, were observed by *in situ* Kerr imaging. Micromagnetic simulations confirm the dendritic domain formation and edge tilting of the magnetisation, as being due to the DMI.

Keywords: spin orbit torque, harmonic measurement, spin-orbit coupling, dendritic domains, *in situ* Kerr measurements

 Supplementary material for this article is available [online](#)

(Some figures may appear in colour only in the online journal)

Introduction

The demand for memory and logic devices [1, 2] has led to significant efforts into the investigation of spintronic material systems. To improve device performance, efforts have been focused on using spin-orbit (SO) effective fields to manipulate magnetization, i.e. in-plane (IP) current induced switching [3–8], fast domain wall (DW) motion [9–11], and magnetic oscillation [12–14]. In heavy metal (HM)/ferromagnetic metal (FM)/oxide trilayer systems, the SO fields generate a SO torque (SOT) which induces spin accumulation via *s* and *d* electrons [15, 16]. Several reports have proposed the underlying mechanism of SOT to be the spin Hall effect (SHE) [4, 5, 10, 16] in bulk HM and at the HM/FM interface to be the

Rashba effect [17–21]. The SO effective fields consists of two components [5, 18, 21–24], i.e. the longitudinal damping-like field (H_L) and the transverse field-like field (H_T) along the $\mathbf{y} \times \mathbf{m}$ direction and \mathbf{y} direction, respectively, where \mathbf{m} and \mathbf{y} are directional unit vectors. The signs of H_L and H_T are dependent on the HM and capping layer thicknesses [22, 25]. In MgO/CoFeB/Ta systems, the coexistence of both the H_L and H_T enables the better study of the effective field components [1] in contrast to Pt-based systems [5, 11].

In this work, *in situ* Kerr imaging was conducted during the harmonic Hall measurements to directly observe the magnetisation behaviour. An analytical energy approach was used to fit the harmonic Hall measurements. This was done by transforming the Hall voltage equation to a field-dependent

equation to determine the coexisting H_L and H_T in a perpendicularly magnetised Ta/MgO/Co₂₀Fe₆₀B₂₀/Ta structure through the second harmonic relation. The dendritic domain width with respect to the applied fields were studied and the strength of the Dzyaloshinskii–Moriya interaction (DMI) for the film was determined. Micromagnetic simulations were conducted to compare with the experimentally determined DMI strength.

Theory

The total magnetic energy in spherical polar coordinates is given by the sum of the contributing energies [26],

$$E_{\text{total}} = (N_z M_s^2 - K_{\perp}) \sin^2 \theta + N_x M_s^2 \cos^2 \theta \sin^2 \varphi + N_y M_s^2 \cos^2 \theta \cos^2 \varphi - M_s H_z \sin \theta - M_s H_y \cos \theta \sin \varphi - M_s H_x \cos \theta \cos \varphi, \quad (1)$$

where $N_z M_s^2 - K_{\perp} \leq 0$, $N_z M_s^2$ is the perpendicular demagnetizing energy density, N_x, N_y, N_z are the demagnetizing factors along the z -, y -, and x -directions respectively, H_x, H_y , and H_z are the applied field components along the three major axes. The Hall voltage measured in the harmonic method includes the anomalous Hall effect (AHE) and planar Hall effect (PHE) when an alternating current with frequency f passes through the nanostructure. The magnetization oscillation due to the SOT can be characterised by $\Delta\theta$ and $\Delta\varphi$. Under the conditions where $\varphi = 0^\circ$ and $\varphi = 90^\circ$, the second harmonic expressions for the longitudinal and transverse schemes can be given by the expressions previously reported in [27] as,

$$V_{2\omega, //} = -\frac{1}{2} I_{\text{ac}} R_{\text{AHE}} \Delta\theta \cos \theta - I_{\text{ac}} R_{\text{PHE}} \Delta\varphi \cos^2 \theta \quad (H \text{ in } x\text{-}z \text{ plane, } \varphi = 0^\circ), \quad (2)$$

$$V_{2\omega, \perp} = -\frac{1}{2} I_{\text{ac}} R_{\text{AHE}} \Delta\theta \cos \theta + I_{\text{ac}} R_{\text{PHE}} \Delta\varphi \cos^2 \theta \quad (H \text{ in } y\text{-}z \text{ plane, } \varphi = 90^\circ), \quad (3)$$

where R_{AHE} and R_{PHE} is the anomalous Hall and planar Hall resistances respectively, and $\Delta\theta$ and $\Delta\varphi$ are the magnetisation oscillations due to the SOT.

The magnetisation oscillations, $\Delta\theta$ and $\Delta\varphi$, were determined at the stable state through the partial derivative of the total energy and can be written as,

$$\Delta\theta_L = -\frac{H_L}{\sqrt{H_k^2 - H_x^2}}; \Delta\varphi_L = -\frac{H_T}{H_x} \quad (\text{longitudinal configuration}), \quad (4)$$

$$\Delta\theta_T = -\frac{H_L}{\sqrt{H_k^2 - H_y^2}}; \Delta\varphi_T = -\frac{H_T}{H_y} \quad (\text{transverse configuration}), \quad (5)$$

where H_L is the longitudinal effective field, H_T the transverse effective field, H_x and H_y are the external magnetic field acting on the system along the x - and y -directions, respectively, and H_k is the effective anisotropic field.

A relationship between V_H and $H_{x(y)}$ was determined using (2)–(5). The harmonic voltage relation with H_x and H_y dependence can be re-expressed as,

$$V_{2\omega, //} = -\frac{I_{\text{ac}} R_{\text{AHE}} H_L}{2H_k} \frac{H_x}{\sqrt{H_k^2 - H_x^2}} + \frac{I_{\text{ac}} R_{\text{PHE}} H_L H_x}{H_k^2}, \quad (6)$$

$$V_{2\omega, \perp} = -\frac{I_{\text{ac}} R_{\text{AHE}} H_T}{2H_k} \frac{H_y}{\sqrt{H_k^2 - H_y^2}} - \frac{I_{\text{ac}} R_{\text{PHE}} H_L H_y}{H_k^2}. \quad (7)$$

The field dependent harmonic relation in (6) and (7) are used to fit the experimental second harmonic signal to determine the effective fields H_L and H_T in both measurement schemes. The above relation assumes that H_L and H_T are constants and independent of magnetisation directions.

Methods

The film consisting of Ta(2 nm)/MgO(2 nm)/CoFeB (1.2 nm)/Ta(5 nm) was deposited on a thermally oxidised SiO_x(300 nm) Si substrate via ultra-high vacuum magnetron sputtering. Post-deposition annealing at 200 °C was conducted on the film for 2 h, to increase strength of the perpendicular magnetic anisotropy. Annealing facilitates the (001) crystalline orientation in the CoFeB layer due to the reorientation of the MgO layer, while Ta provides a sink for the diffusion of B atoms [28]. The film was measured to have high resistivity (181 $\mu\Omega$ cm), which indicates that Ta largely grows in the β -phase, which is commonly reported to have a large spin Hall angle [4]. The film was patterned into a symmetrical Hall cross with a width of 5 μm using electron beam lithography and ion milling techniques. The magnetic properties of the film were determined using a vibrating sample magnetometer with an applied field oriented out-of-plane (OOP) and IP to the film plane. The film has a saturation magnetisation, $M_s = 1.4 \times 10^6$ A m⁻¹ and an effective anisotropic field, $H_k = 3.84$ kOe.

Results and discussion

A custom-built Kerr imaging system [29–31] was used to observe the magnetisation behaviour of the thin film and the Hall cross *in situ*. The magnetisation reversal of the Hall cross was observed to be initiated by nucleation at specific sites, followed by dendritic growth and the expansion of the domains. The growth of the dendritic domains during an OOP field sweep is shown in supplementary video 1 (stacks.iop.org/JPhysD/51/115004/mmedia). The unreversed magnetisation between the dendritic branches diminishes until an additional field was applied to overcome the energy barrier, thus leading to a non-sharp switching before reaching saturation [32]. The AHE [33] measurement in figure 1(a) shows that the Hall cross patterned film structure has coercivity, $H_c = 25$ Oe, and anomalous Hall resistance $R_{\text{AHE}} = 0.68$ Ω when the field was swept along the OOP direction with a non-perturbing measurement current density of 7.5×10^4 A cm⁻².

The domain width of the demagnetised state of the sample was analysed using a Kerr microscope. An OOP magnetic field of 200 Oe was applied to saturate the sample and then

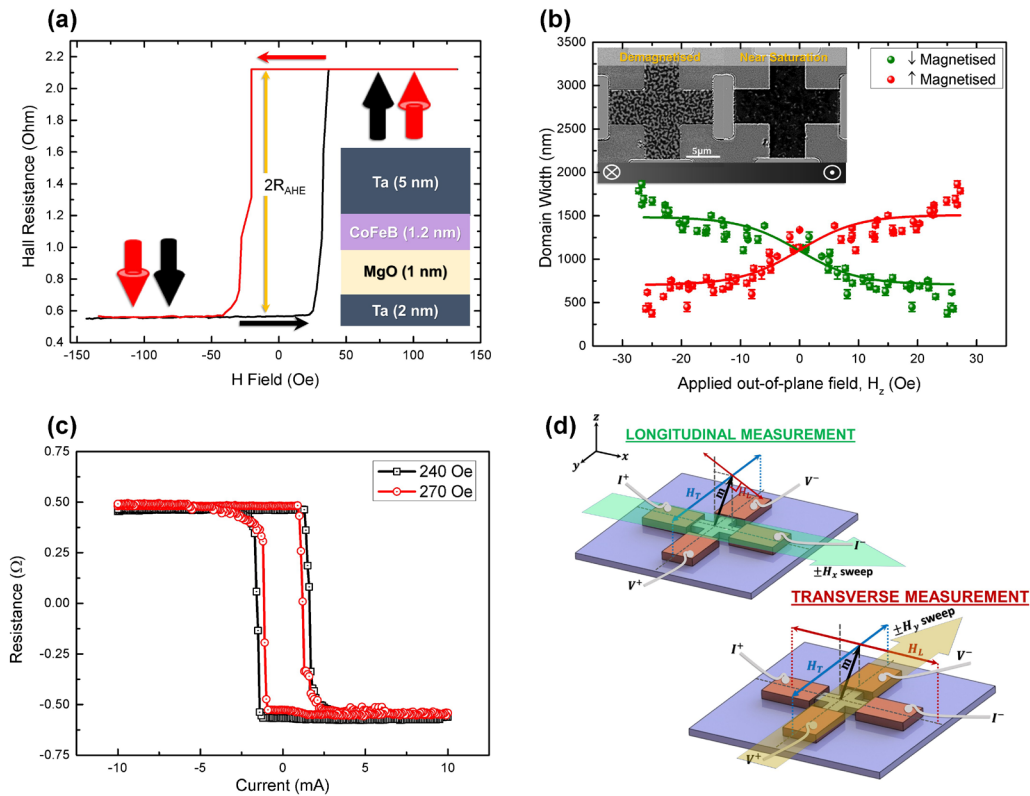


Figure 1. (a) Anomalous Hall resistance R_{AHE} as a function of H applied in the OOP direction at 300 K. (b) Dendritic domain width (up and down domains) variation as a function of the applied OOP field, with a differential Kerr image of magnetic dendritic domains of the film stack [Ta(2 nm)/MgO(2 nm)/CoFeB (1.2 nm)/Ta(5 nm)] in a $5 \mu\text{m}$ width Hall cross in a demagnetised state and approaching the saturation state (inset). The error bars denote the standard deviation from ten individual domain width determinations. (c) Current-induced switching of the film stack at a fixed IP-field of 240 and 270 Oe. (d) Schematic of longitudinal and transverse measurement scheme for the symmetrical Hall cross in Cartesian coordinate geometry indicating the $H_{x(y)}$ sweep, effective fields, H_L and H_T , with respect to the IP current for a MgO/CoFeB/Ta nanowire.

the applied field was gradually decreased until a demagnetised state showing dendritic domains was observed as shown in the inset of figure 1(b). Subsequently, the dendritic domain width was measured as a function of the OOP field as shown in figure 1(b). As the field is increased in the positive direction, the width of the up domains (black) expands until the down domains (white) annihilate near saturation. In earlier reports, the maximum field in which the domains still exist can be used to determine the DMI [34, 35]. The field evolution of the dendritic domains leads to a hysteresis like curve in figure 1(b). A hyperbolic tangent function, $w(H) = a \cdot \tanh(\delta \cdot H + \phi) + d$ [36, 37], was utilised to determine the terminal width, $w_{\text{term}} = 700 \pm 80 \text{ nm}$, just before the annihilation of the dendrites and the average periodicity of $w_{\text{average}} = 1200 \pm 80 \text{ nm}$. In a multi-domain state, the domain width provides a means of quantifying the DMI through established models [38]. The DMI strength, D , was determined through the DW surface energy density, $\sigma_{\text{DW}} = 4\sqrt{AK_{\text{eff}}} - \pi|D|$, where A is the exchange stiffness, K_{eff} is the uniaxial effective anisotropy constant, and D is the DMI constant. The presence of the DMI, $|D| = 0.65 \pm 0.08 \text{ mJ m}^{-2}$, enables the stabilisation of the dendritic domains in the demagnetised state. The $|D|$ was determined throughout the regions with dendritic domains, inclusive of pinning sites within the Hall wire which gave rise to the DMI error. To ensure comparability with spin-transfer

torque (STT) critical current densities, current pulses were used to induce magnetisation switching in the Hall cross with an applied IP field of 240 Oe as shown in figure 1(c). The critical switching current was 1.5 mA ($1.35 \times 10^6 \text{ A cm}^{-2}$) which is comparable to the critical switching current density for STT [39]. The SO effective fields were subsequently quantified through *in situ* Kerr harmonic measurements and the scheme of these measurements are illustrated in figure 1(d).

MuMax³ micromagnetic simulation [40] was conducted to verify that the dendritic domains related to the DMI. The relaxed demagnetised state of the Hall bar was simulated using DMI values ranging from 0–2.9 mJ m^{-2} in steps of 0.1. In the numerical simulations, the device has geometrical dimensions of $5 \mu\text{m}$ width \times $10 \mu\text{m}$ length, K_u of $2.72 \times 10^5 \text{ J m}^{-3}$, M_s of $1.4 \times 10^6 \text{ A m}^{-1}$, and exchange stiffness, A_{ex} of $2 \times 10^{-11} \text{ J m}^{-1}$ [22]. The domain width spacing as a function of the DMI was determined as shown in figure 2(a). At $D = 0 \text{ mJ m}^{-2}$, the sample forms larger sized domains and with increasing value of D , the domains shrink exponentially in size. By utilising the simulated relation between domain width and the DMI, the DMI for a demagnetised domain width of $1130 \pm 40 \text{ nm}$ corresponds to $|D| = 0.6 \text{ mJ m}^{-2}$. The simulated results agree with the experimentally determined DMI. The presence of the DMI in CoFeB/Ta allows the conclusion that post deposition thin film leads to improvements in atomic ordering at the

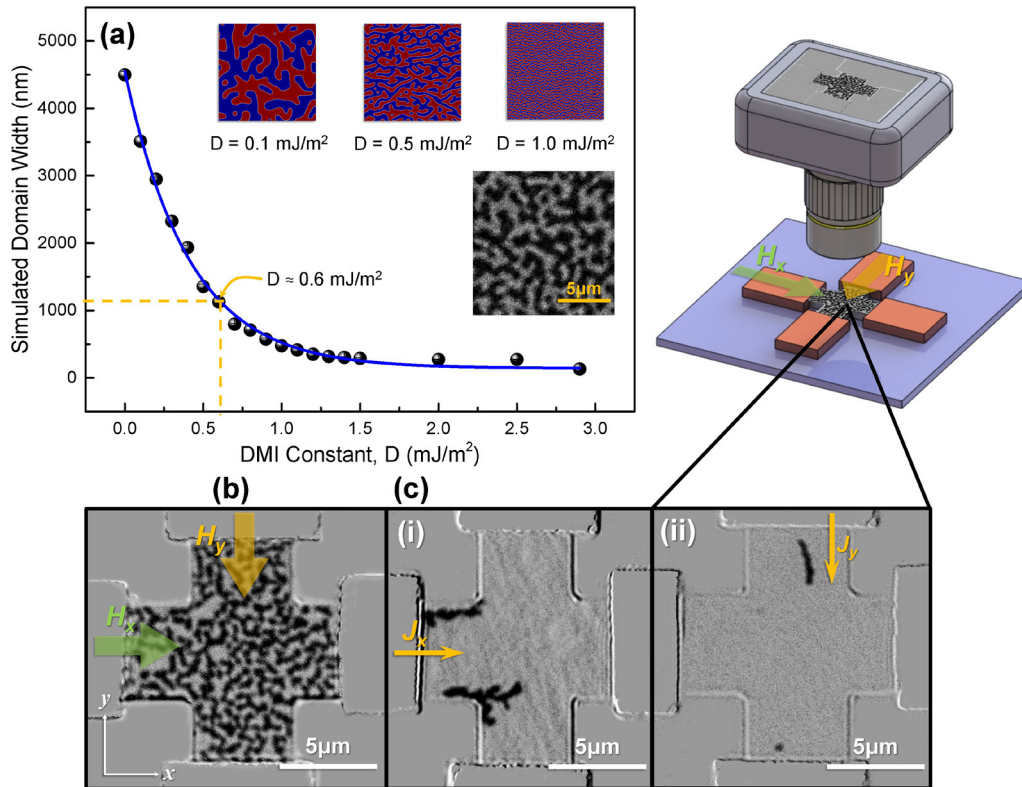


Figure 2. (a) Domain width as a function of DMI strength, $|D|$ from numerical simulations with inset snapshots of the dendritic domains at various values of $|D|$ and the *in situ* Kerr image of the centre of the Hall cross in the demagnetised state. Observation of the (b) field induced nucleation of dendritic domains when a pulsed field of 1.2 kOe was applied, and (c) domain creep when $I_{ac} = 1 \times 10^{11} \text{ A m}^{-2}$ was applied in the (i) x -direction (ii) and y -direction, respectively.

CoFeB/Ta interface which strengthened the DMI between the Ta and CoFeB layers [41, 42].

In situ Kerr harmonic Hall measurement

Before the addition of the sinusoidal alternating current, field induced, and current induced nucleation were observed separately as shown in figures 2(b) and (c), respectively. The nucleation of dendritic domains appears spontaneously at various spots on the Hall cross as the IP-field was swept through zero. The DMI in the sample manifests itself by stabilising the dendritic texture in the Hall cross [43]. Furthermore, the DMI leads to tilting of magnetisation at the edges leading to nucleation and expansion from the edge of the Hall cross device. At a 1.2 kOe pulsed IP-field, dendritic domains formed are as shown in figure 2(b). When I_{AC} was applied in the x and y regime without an IP-field for a period of 5 min, creeping domain nucleation occur near the contacts and enlarges in an elongated manner in the x and y directions as shown in figure 2(c). The current-induced nucleation was due to the spin Hall torque on the magnetisation in the Hall cross.

In the *in situ* Kerr harmonic measurement, dendritic domains are nucleated and progressively expands and contracts with a sweeping IP-field as shown in supplementary video 2. Figure 3 shows snapshots of the Hall cross magnetisation behaviour at different applied magnetic fields when current was applied to the sample. The current dependence of the effective field was determined by varying the sinusoidal

input current I_{AC} with the reference frequency of 307.1 Hz. The current densities were modulated with a step size of $1 \times 10^{10} \text{ A m}^{-2}$ from $1 \times 10^{10} \text{ A m}^{-2}$ to $1 \times 10^{11} \text{ A m}^{-2}$. The first and second harmonic voltages (V_{ω} and $V_{2\omega}$ respectively) were measured simultaneously and averaged over 120 readings per data point for a better sound to noise ratio. Two measurement schemes, i.e. longitudinal measurement where the applied current and field are in the same direction and transverse measurement where the applied current and field are orthogonal to each other, were performed separately. The observation shown in figure 3 proves the hysteresis behaviour in the first harmonic voltage, as the CoFeB layer switches partially, forming dendritic domains which grows with respect to the applied IP field.

The current dependence of the harmonic results for both the longitudinal and transverse measurements are shown in figures 4(a)–(d). In the longitudinal measurement, the first harmonic signals show hysteresis like loops, indicating the presence of domain nucleation and expansion. At a low applied IP-field, a small number of domains still exist. They are randomly moving and are spread out in the Hall cross shown in supplementary video 2. The second harmonic signals reveal asymmetric wave-like patterns about the vertical axes. The rise to the peak, $V_{2\omega, \text{peak}}$ is characterised by the formation of dendritic domains as observed in the first harmonic signal. The corresponding field, H_{peak} at the asymmetric peaks, $V_{2\omega, \text{peak}}$, is related to the effective anisotropy field, H_k of CoFeB and the effective fields acting on the CoFeB. With the increase

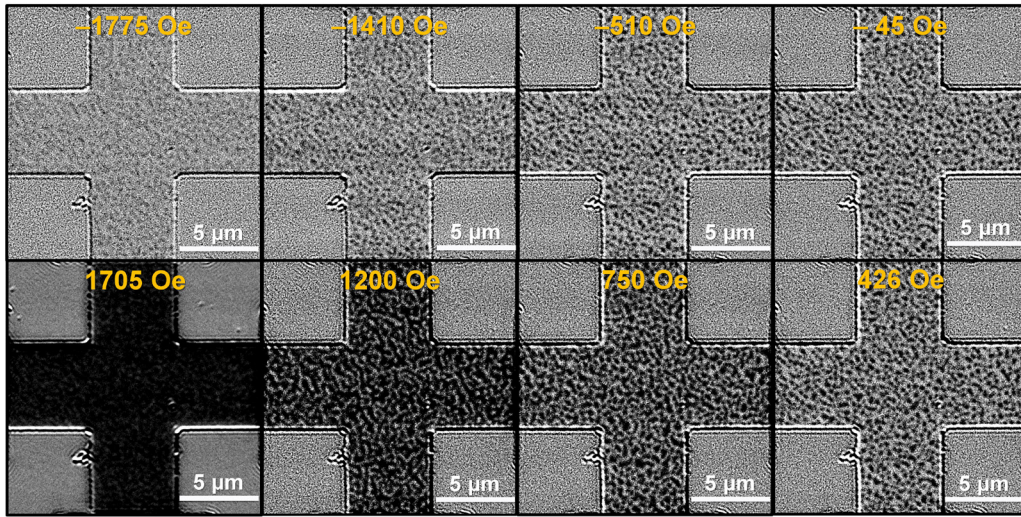


Figure 3. *In situ* Kerr observation of the progressive nucleation and expansion of dendritic domains, when an IP magnetic field is applied during the longitudinal and transverse harmonic measurement scheme observed under the custom-built Kerr microscope.

of the current density, the H_{peak} decreases monotonically with the applied current density as shown in the inset of figure 4(a). This occurs as the applied current together with the external IP field facilitates the depinning of the domains at various sites, favouring domain expansion. As the current increases, energy is supplied to overcome the pinning field, hence we observe an inward shift in the H_{peak} as shown by the dotted line in figure 4(b). In the transverse measurement scheme, a symmetrical dip about the vertical axis was observed and flattens out when the magnetization state changes. Nucleation and expansion of the dendritic domains occur in a similar manner as the longitudinal measurement scheme observed through the hysteresis in the first harmonic as shown in figure 4(c). The slope of the transverse curve rises till saturation, indicating the expansion of the domains as the IP field increases. In both measurement schemes, the measured domain width for both measurement schemes are as shown in the inset of figure 4(d). The up magnetised domains (black) increases in width as the field is swept in the positive x -direction and the down magnetised domains (white) increases in width as the field is swept in the opposite direction. The change in domain width for both field sweep directions corresponds to 1100 ± 300 nm.

Assuming H_L and H_T are constants, the derived equation was used to fit the experimental results within $-1.1 \text{ kOe} \leq H_{x(y)} \leq 1.1 \text{ kOe}$. The device has known parameters of $R_{\text{AHE}} = 1.35 \Omega$ and $R_{\text{PHE}} = 0.97 \Omega$. Equations (6) and (7) were used to experimentally fit the curve as shown in figures 5(a) and (b) for the longitudinal and transverse measurement schemes, respectively, by utilising the second harmonic signal. The effective field in the longitudinal scheme was determined to be $H_L = -12 \text{ Oe}$ and $H_T = 8 \text{ Oe}$ per 10^6 A cm^{-2} with $H_k = 3.84 \text{ kOe}$. In the transverse scheme, $H_L = -12 \text{ Oe}$ and $H_T = -17 \text{ Oe}$ per 10^6 A cm^{-2} . The inclusion of the PHE is necessary to attain a sufficiently accurate value of H_L and H_T . The values determined are larger than earlier reports. Several reports have shown that the H_L arises due to the SHE [5, 10, 44] while H_T arises due to the Rashba effect [3, 8, 9, 18, 21]. Assuming that the SHE is

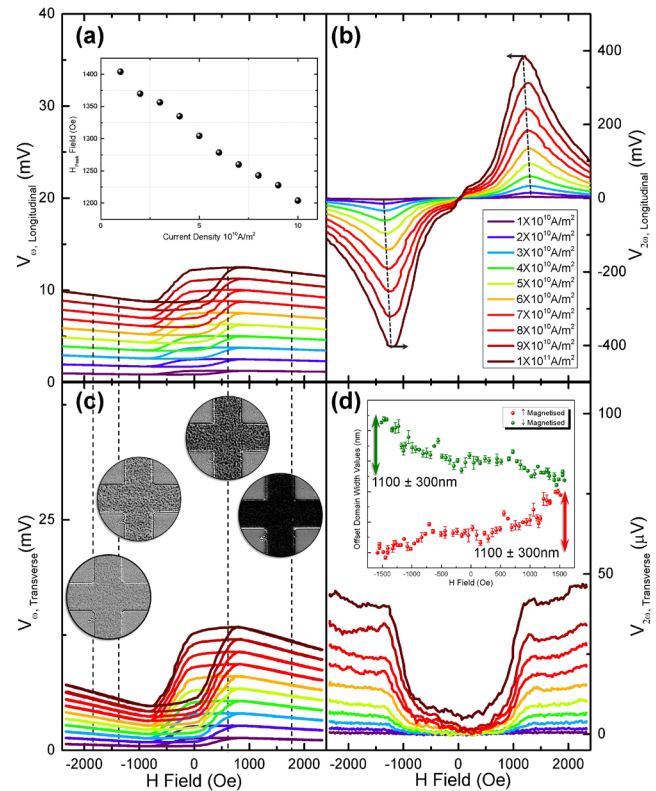


Figure 4. *In situ* harmonic Hall measurement. Current dependence in the longitudinal measurement scheme of the (a) first harmonic and the peak shift of the second harmonics as a function of the applied current density (inset) and (b) second harmonic measured at $\theta_H = 4^\circ$ at 300 K. Current dependence in the transverse measurement scheme of the (c) first harmonic and (d) second harmonic measured at $\theta_H = 4^\circ$ at 300 K and the domain width as a function of the applied field before the complete annihilation of the dendritic domains (inset). Domain structure at different field values are shown on the first harmonics for both the longitudinal and transverse measurement schemes.

largely contributing to give rise to H_L , the parameters θ_{SH} and H_L can be related by, $H_L = \hbar\theta_{\text{SH}} |j_e|/2 |e| M_s t_f$, where

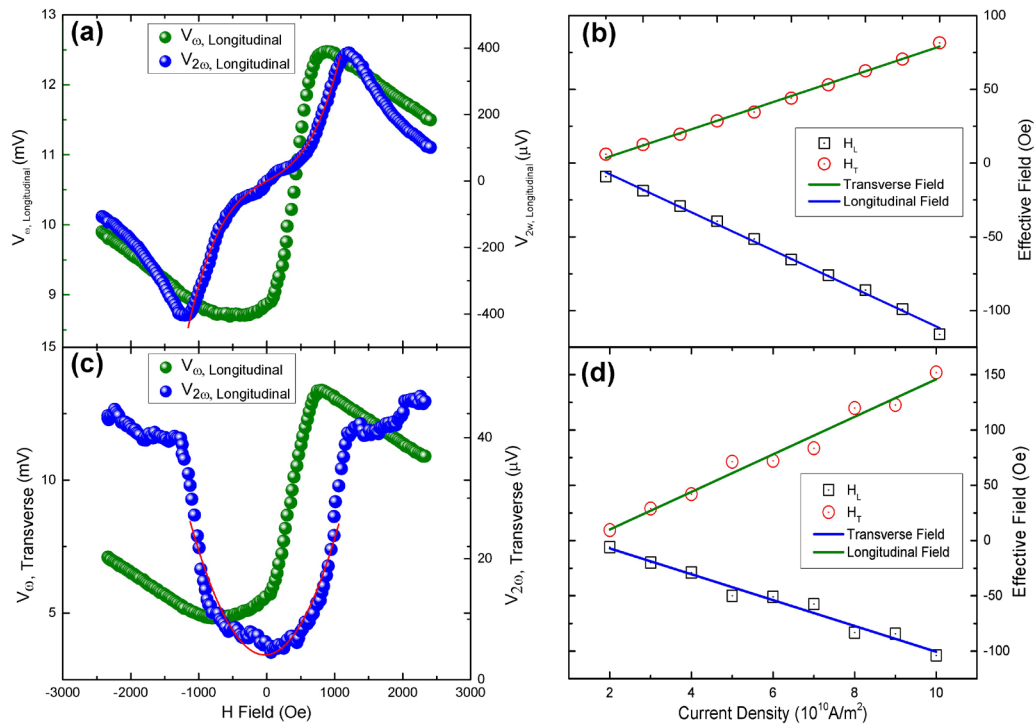


Figure 5. (a), (c) Experimental fitting of the second harmonic voltages shown together with the first harmonic signal. The fitted H_L and H_T are calculated from the fitting (red curve). (b) Current dependence of the longitudinal and transverse SO effective field following the current density values ranging from $1 \times 10^{10} \text{ A m}^{-2}$ to $1 \times 10^{11} \text{ A m}^{-2}$ for the longitudinal measurement scheme, (d) the transverse measurement scheme.

$M_s = 1.4 \times 10^6 \text{ A m}^{-1}$, t_f is the ferromagnetic thickness. The spin Hall angle was determined to be $\theta_{\text{SH}}^{\text{Ta}} \approx -0.14 \pm 0.05$ and is similar to earlier reports at 300 K [4]. The current-induced effective fields are strongly correlated to the current density as indicated in figures 5(c) and (d). The longitudinal effective field, H_L , in both the longitudinal and transverse measurement schemes shows clear monotonic behaviour with increasing current density. This is mainly caused by the SHE [23, 45]. The determination of H_T was through the PHE term in the derived equation, and we conclude that significant PHE was present in CoFeB (R_{PHE}) that gave rise to the large coexistence of the H_T . The magnitude of H_T is smaller than H_L , as the bulk SHE dominates in the longitudinal measurement scheme [4].

Conclusion

In conclusion, we have observed dendritic domain expansion in the IP harmonic Hall measurement via *in situ* Kerr imaging. Interfacial DMI in the CoFeB/Ta layer was responsible for the domain dynamics during the measurement, which was affirmed through micromagnetic simulation. The coexisting H_L and H_T was determined through the analytical energy approach at varying current densities at low frequency. The longitudinal scheme has $H_L = -12 \text{ Oe}$ and $H_T = 8 \text{ Oe}$ per 10^6 A cm^{-2} and the transverse scheme has $H_L = -12 \text{ Oe}$ and $H_T = -17 \text{ Oe}$ at 10^6 A m^{-2} , with a spin Hall angle of $\theta_{\text{SH}}^{\text{Ta}} \approx -0.14 \pm 0.05$. The perpendicularly magnetised MgO/

CoFeB/Ta film exhibited the coexistence of H_L and H_T due to the large PHE contribution. Our results reveal that the magnetisation reversal is achieved via the formation and expansion of a dendritic domain which is responsible for the effective fields determined.

Acknowledgments

This work was supported by the Singapore National Research Foundation, Prime Minister's Office under a Competitive Research Programme (Non-volatile Magnetic Logic and Memory Integrated Circuit Devices, NRF-CRP9-2011-01), and an Industry-IHL Partnership Program (NRF2015-IIP001-001). The support from an RIE2020 AME-Programmatic Grant (No. A1687b0033) is also acknowledged. WSL is also a member of the Singapore Spintronics Consortium (SG-SPIN).

ORCID iDs

Q Y Wong <https://orcid.org/0000-0002-6761-423X>
 W L Gan <https://orcid.org/0000-0001-9278-0718>
 G J Lim <https://orcid.org/0000-0003-2411-5841>
 C C I Ang <https://orcid.org/0000-0001-9479-7011>
 F N Tan <https://orcid.org/0000-0002-9646-2466>
 W C Law <https://orcid.org/0000-0002-1572-6694>
 W S Lew <https://orcid.org/0000-0002-5161-741X>

References

- [1] Garello K *et al* 2013 Symmetry and magnitude of spin-orbit torques in ferromagnetic heterostructures *Nat. Nanotechnol.* **8** 587–93
- [2] Cubukcu M *et al* 2014 Spin-orbit torque magnetization switching of a three-terminal perpendicular magnetic tunnel junction *Appl. Phys. Lett.* **104** 042406
- [3] Miron I M *et al* 2011 Perpendicular switching of a single ferromagnetic layer induced by in-plane current injection *Nature* **476** 189–93
- [4] Liu L *et al* 2012 Spin-torque switching with the giant spin Hall effect of tantalum *Science* **336** 555–8
- [5] Liu L *et al* 2012 Current-induced switching of perpendicularly magnetized magnetic layers using spin torque from the spin Hall effect *Phys. Rev. Lett.* **109** 096602
- [6] Fan X *et al* 2013 Observation of the nonlocal spin-orbital effective field *Nat. Commun.* **4** 1799
- [7] Avci C O *et al* 2012 Magnetization switching of an MgO/Co/Pt layer by in-plane current injection *Appl. Phys. Lett.* **100** 212404
- [8] Suzuki T *et al* 2011 Current-induced effective field in perpendicularly magnetized Ta/CoFeB/MgO wire *Appl. Phys. Lett.* **98** 142505
- [9] Miron I M *et al* 2011 Fast current-induced domain-wall motion controlled by the Rashba effect *Nat. Mater.* **10** 419–23
- [10] Emori S *et al* 2013 Current-driven dynamics of chiral ferromagnetic domain walls *Nat. Mater.* **12** 611–6
- [11] Emori S, Bono D C and Beach G S 2012 Interfacial current-induced torques in Pt/Co/GdO_x *Appl. Phys. Lett.* **101** 042405
- [12] Demidov V E *et al* 2012 Magnetic nano-oscillator driven by pure spin current *Nat. Mater.* **11** 1028–31
- [13] Liu L *et al* 2012 Magnetic oscillations driven by the spin Hall effect in 3-terminal magnetic tunnel junction devices *Phys. Rev. Lett.* **109** 186602
- [14] Liu R, Lim W and Urazhdin S 2013 Spectral characteristics of the microwave emission by the spin Hall nano-oscillator *Phys. Rev. Lett.* **110** 147601
- [15] Zhang S, Levy P and Fert A 2002 Mechanisms of spin-polarized current-driven magnetization switching *Phys. Rev. Lett.* **88** 236601
- [16] Tserkovnyak Y, Brataas A and Bauer G E 2008 Theory of current-driven magnetization dynamics in inhomogeneous ferromagnets *J. Magn. Magn. Mater.* **320** 1282–92
- [17] Haazen P *et al* 2013 Domain wall depinning governed by the spin Hall effect *Nat. Mater.* **12** 299–303
- [18] Miron I M *et al* 2010 Current-driven spin torque induced by the Rashba effect in a ferromagnetic metal layer *Nat. Mater.* **9** 230–4
- [19] Pesin D and MacDonald A 2012 Quantum kinetic theory of current-induced torques in Rashba ferromagnets *Phys. Rev. B* **86** 014416
- [20] Kim K-W *et al* 2012 Magnetization dynamics induced by in-plane currents in ultrathin magnetic nanostructures with Rashba spin-orbit coupling *Phys. Rev. B* **85** 180404
- [21] Wang X and Manchon A 2012 Diffusive spin dynamics in ferromagnetic thin films with a Rashba interaction *Phys. Rev. Lett.* **108** 117201
- [22] Kim J *et al* 2013 Layer thickness dependence of the current-induced effective field vector in Ta/CoFeB/MgO *Nat. Mater.* **12** 240–5
- [23] Jamali M *et al* 2013 Spin-orbit torques in Co/Pd multilayer nanowires *Phys. Rev. Lett.* **111** 246602
- [24] Seo S-M *et al* 2012 Current-induced motion of a transverse magnetic domain wall in the presence of spin Hall effect *Appl. Phys. Lett.* **101** 022405
- [25] Sethi P *et al* 2017 Modulation of spin-orbit torque efficiency by thickness control of heavy metal layers in Co/Pt multilayers *J. Magn. Magn. Mater.* **426** 497–503
- [26] Hayashi M *et al* 2014 Quantitative characterization of the spin-orbit torque using harmonic Hall voltage measurements *Phys. Rev. B* **89** 144425
- [27] Qiu X *et al* 2014 Angular and temperature dependence of current induced spin-orbit effective fields in Ta/CoFeB/MgO nanowires *Sci. Rep.* **4** 4491
- [28] Alzate J G *et al* 2014 Temperature dependence of the voltage-controlled perpendicular anisotropy in nanoscale MgO/CoFeB/Ta magnetic tunnel junctions *Appl. Phys. Lett.* **104** 112410
- [29] Engel C *et al* 2017 Spin-orbit torque induced magnetization anisotropy modulation in Pt/(Co/Ni)₄/Co/IrMn heterostructure *J. Appl. Phys.* **121** 143902
- [30] Li S *et al* 2017 Deterministic spin-orbit torque induced magnetization reversal in Pt/[Co/Ni] n/Co/Ta multilayer Hall bars *Sci. Rep.* **7** 972
- [31] Ramu M *et al* 2017 Spin orbit torque induced asymmetric depinning of chiral Néel domain wall in Co/Ni heterostructures *Appl. Phys. Lett.* **110** 162402
- [32] Liu H-L *et al* 2011 Direct observation of dendritic domain growth in perpendicular magnetic anisotropy CoFe/Pt multilayers *J. Magn. Magn. Mater.* **323** 2238–42
- [33] Nagaosa N *et al* 2010 Anomalous Hall effect *Rev. Mod. Phys.* **82** 1539–92
- [34] Woo S *et al* 2016 Observation of room-temperature magnetic skyrmions and their current-driven dynamics in ultrathin metallic ferromagnets *Nat. Mater.* **15** 501–6
- [35] Jaiswal S *et al* 2017 Investigation of the Dzyaloshinskii–Moriya interaction and room temperature skyrmions in W/CoFeB/MgO thin films and microwires *Appl. Phys. Lett.* **111** 022409
- [36] Litzius K *et al* 2016 Skyrmion Hall effect revealed by direct time-resolved x-ray microscopy *Nat. Phys.* **13** 170–5
- [37] Takács J 2001 A phenomenological mathematical model of hysteresis *COMPEL, Int. J. Comput. Math. Electr. Electron. Eng.* **20** 1002–15
- [38] Málek Z and Kamberský V 1958 On the theory of the domain structure of thin films of magnetically uni-axial materials *Czechoslovakij Fiziceskij Z.* **8** 416–21
- [39] Ikeda S *et al* 2010 A perpendicular-anisotropy CoFeB–MgO magnetic tunnel junction *Nat. Mater.* **9** 721–4
- [40] Vansteenkiste A *et al* 2014 The design and verification of MuMax3 *AIP Adv.* **4** 107133
- [41] Lo Conte R *et al* 2015 Role of B diffusion in the interfacial Dzyaloshinskii–Moriya interaction in Ta/Co₂₀Fe₆₀B₂₀/MgO nanowires *Phys. Rev. B* **91** 014433
- [42] Torrejon J *et al* 2014 Interface control of the magnetic chirality in CoFeB/MgO heterostructures with heavy-metal underlayers *Nat. Commun.* **5** 4655
- [43] Han D S *et al* 2016 Asymmetric hysteresis for probing Dzyaloshinskii–Moriya interaction *Nano Lett.* **16** 4438–46
- [44] Haney P M *et al* 2013 Current-induced torques and interfacial spin-orbit coupling *Phys. Rev. B* **88** 214417
- [45] Avci C O *et al* 2014 Fieldlike and antidamping spin-orbit torques in as-grown and annealed Ta/CoFeB/MgO layers *Phys. Rev. B* **89** 214419